

Homogeneous Electrocatalytic Reduction of CO₂ by a CrN₃O Complex: Electronic Coupling with Redox-Active Terpyridine Fragment Favors Selectivity for CO

Shelby L. Hooe, Juan J. Moreno, Diane A. Dickie, and Charles W. Machan*

* - machan@virginia.edu; ORCID 0000-0002-5182-1138

S.L.H. ORCID 0000-0002-6991-2273; J.J.M. ORCID 0000-0003-1809-6170; D.A.D. ORCID 0000-0003-0939-3309

Department of Chemistry, University of Virginia, PO Box 400319, Charlottesville, VA 22904-4319

Abstract

Electrocatalyst design and optimization strategies continue to be an active area of research interest for the applied use of renewable energy resources and the development of associated technologies. The electrocatalytic conversion of CO₂ is an attractive approach in this context, because of the added potential benefit of addressing its rising atmospheric concentrations. In previous experimental and computational studies we have described the mechanism of the first molecular Cr complex capable of electrocatalytically reducing CO₂ to CO in the presence of an added proton donor, which contained a redox-active 2,2'-bipyridine (bpy) fragment, CrN₂O₂. The high selectivity for CO in the bpy-based system was dependent on a delocalized Cr(II)(bpy^{•-}) active state. Subsequently, we became interested in exploring how expanding the polypyridyl ligand core would impact selectivity and activity during electrocatalytic CO₂ reduction. Here, we report a new CrN₃O catalyst, Cr(tpy^{tbu}pho)Cl₂ **1**, where 2-([2,2':6',2''-terpyridin]-6-yl)-4,6-di-tert-butylphenolate = [tpy^{tbu}pho]⁻, which reduces CO₂ to CO with quantitative selectivity *via* a different mechanism than our previously reported Cr(^{tbu}dhbpy)Cl(H₂O) catalyst. Computational analyses indicate that changes in the overall reaction are the combined result of a decrease in intrinsic ligand charge (L₃X vs L₂X₂) and an increase in ligand redox activity, which result in increased electronic coupling between the doubly reduced tpy fragment of the ligand and a Cr(II) center.

Introduction

Rising concerns over increasing energy demands and global climate change have led to continued interest in the development of molecular catalysts capable of interconverting electrical and chemical energy.¹⁻³ Specifically, the electrocatalytic reduction of carbon dioxide (CO₂) to carbon monoxide (CO) using renewable energy⁴⁻⁶ represents a potentially valuable pathway to the synthesis of liquid fuels via the Fischer-Tropsch process,⁷ in the manufacturing of acetic acid,⁸ and in hydroformylation reactions.⁹ In homogeneous electrocatalysis for CO₂ reduction, the Cr/Mo/W triad is underrepresented,⁴⁻⁶ with a limited number of reports of systems which are electrochemically or electrocatalytically active, few of which exhibit stability during electrolysis.¹⁰⁻¹⁷

Previously we reported the first homogeneous Cr electrocatalyst for quantitative CO₂ reduction to CO, Cr(^tbu₄dhbpy)Cl(H₂O), where 6,6'-di(3,5-di-*tert*-butyl-2-phenolate)-2,2'-bipyridine = [^tbu₄dhbpy]²⁻.¹⁸⁻²⁰ We proposed a catalytic mechanism for the Cr(^tbu₄dhbpy)Cl(H₂O) catalyst whereby C–OH bond cleavage was the rate-determining step, based on mechanistic and computational studies. The noteworthy kinetic selectivity of this complex for CO was ascribed to the electronic structure of the catalytically active species: a square planar [Cr(II)(^tbu₄dhpy^{•-})]⁻ species (**Figure 1**) that exhibited anti-ferromagnetic coupling between a bpy-based radical anion and the Cr(II) center (*S* = 3/2). Based on previous reports about the role of electronic coupling in driving selectivity,²¹⁻²⁷ we reasoned that the redox activity of our bpy-based ligand could be translated to expanded polypyridyl ligand frameworks to examine how electronic coupling between Cr and the reduced ligand frameworks impacts catalytic performance. This was motivated by the known role of electronic coupling between 2,2':6',2''-terpyridine (tpy) fragments or 2,2':6',2'':6'',2'''-

quaterpyridine (qpy) and later transition metals like Fe^{23-24, 27} or Co²⁷ in achieving high selectivity and activity at low overpotentials.

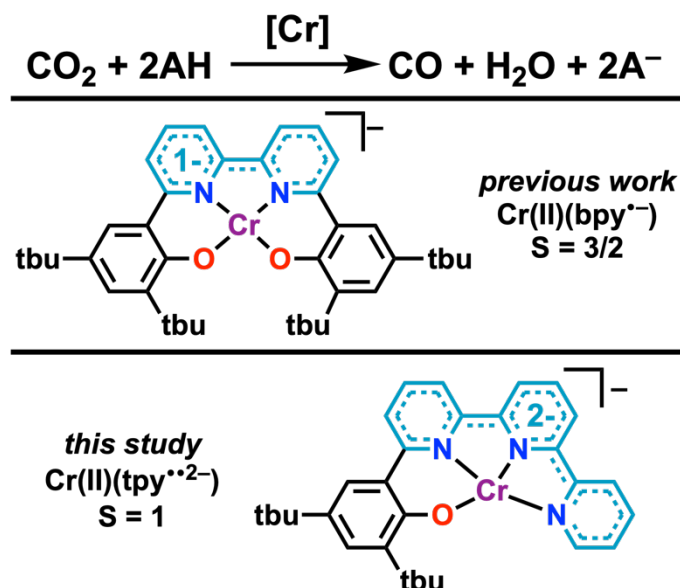


Figure 1. A comparison of the electronic structure of the active states for bpy- and tpy-based Cr complexes capable of mediating homogeneous electrocatalytic CO₂ reduction to CO.

Here we present a new molecular Cr catalyst, Cr(tpy^{tbu}pho)Cl₂ **1**, where 2-([2,2':6',2''-terpyridin]-6-yl)-4,6-di-tert-butylphenolate = [tpy^{tbu}pho]⁻, which exhibits activity for CO₂ reduction to CO via a different mechanism relative to our initial Cr(^{tbu}dhbpy)Cl(H₂O) catalyst. Experimental and computational analyses reveal the new Cr(tpy^{tbu}pho)Cl₂ **1** electrocatalyst operates with important differences in the overall mechanism, which arises from the expanded redox activity of the tpy fragment relative to bpy, achieving an active state best described as [Cr(II)(tpy^{tbu}pho^{••})]⁻ (**Figure 1**). Interestingly, these results also reveal that the charge of the supporting ligand plays an important role, since the benefit of expanded redox activity in [tpy^{tbu}pho]⁻ appears to be balanced by the shift from a L₂X₂ coordination environment to L₃X. This study suggests that Cr electrocatalysts for CO₂ reduction can benefit from ligand design strategies that have previously been explored only for later transition metals and carbonyl-containing complexes.

Results and Discussion

The synthesis of 2-([2,2':6',2''-terpyridin]-6-yl)-4,6-di-*tert*-butylphenol, [tpy^{tbu}phoH]⁰, was achieved via an initial coupling of 2,6-dibromopyridine to 2,2'-bipyridine to make 6-bromo-2,2':6',2''-terpyridine.²⁸ Subsequent microwave-assisted Suzuki-type cross-coupling of 6-bromo-2,2':6',2''-terpyridine with (3,5-di-*tert*-butyl-2-hydroxy-phenyl)boronic acid¹⁸ produced [tpy^{tbu}pho(H)]⁰ in high yield. The Cr(tpy^{tbu}pho)Cl₂ **1** complex was synthesized in a similar manner to our previous report (See **Materials and Methods** Section of SI for detailed procedures).¹⁸ Both [tpy^{tbu}pho(H)]⁰ and **1** were characterized via HRMS, EA, NMR, and UV-vis spectroscopies (SI **Materials and Methods** Section, **Table S1**, and **Figures S1-S5**). The proposed molecular connectivity was supported by structural data obtained from single-crystal X-ray diffraction studies (**Figure 2**).

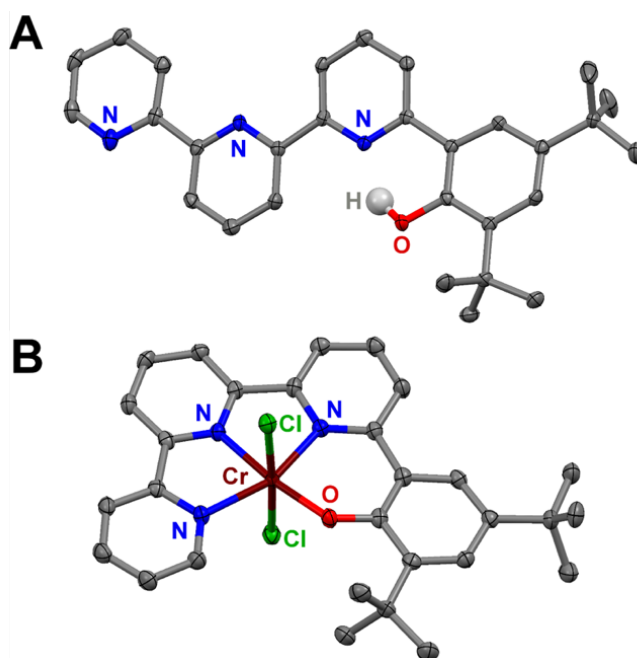


Figure 2. (A) Molecular structure of [tpy^{tbu}phoH]⁰ obtained from single-crystal X-ray diffraction studies. All non-phenolate H atoms removed for clarity. Crystals were grown by slow cooling a saturated hexane solution of the ligand. (B) Molecular structure of Cr(tpy^{tbu}pho)Cl₂ **1** obtained from single-crystal X-ray diffraction studies. Crystals were grown from slow evaporation of a DCM/MeCN mixture at room temperature. H atoms and MeCN molecule omitted for clarity. Blue = N, red = O, gray = C, green = Cl, maroon = Cr, white = H atoms; thermal ellipsoids at 50%.

Cyclic voltammetry experiments were performed on $\text{Cr}(\text{tpy}^{\text{tbu}}\text{pho})\text{Cl}_2$ **1** in a solution of 0.1 M tetrabutylammonium hexafluorophosphate (TBAPF_6) in N,N -DMF. Under argon (Ar) saturation conditions **1** displays three redox features at potentials more negative than the ferrocenium/ferrocene (Fc^+/Fc) redox couple: $E_p = -1.46$ V, $E_{1/2} = -1.64$ V, and $E_{1/2} = -2.18$ V versus Fc^+/Fc (**Figure 3**, black and **Figure S6**). A small wave is observed at -1.85 V, following the second reduction, which we propose relates to equilibria involving solvent displacement of bound Cl^- at Cr. This proposal is supported by CV data obtained with tetrabutylammonium chloride (TBACl) present as a source of excess Cl^- anions (**Figures S7 and S8**). Under Ar saturation conditions with added TBACl, only three reduction waves are observed and there is a shift towards more negative potentials for all three reductions of $\text{Cr}(\text{tpy}^{\text{tbu}}\text{pho})\text{Cl}_2$ relative to identical conditions in the absence of TBACl. These data suggest that overall, the complex undergoes three one-electron reduction events in the observed potential window, *vide infra*.

Upon the addition of 0.1 M phenol (PhOH) under Ar saturation conditions, minimal shifts in the first two redox features of **1** are observed, but the third redox feature displays a slight increase in current with some loss of reversibility (**Figure 3**, green). In the absence of an added proton donor under CO_2 saturation conditions, CV data indicates CO_2 binding occurs: a pre-wave is observed at -2.13 V versus Fc^+/Fc , slightly positive of the third reduction of $\text{Cr}(\text{tpy}^{\text{tbu}}\text{pho})\text{Cl}_2$ (**Figure 3**, red). The slight increase in current and loss of reversibility at the third reduction under aprotic conditions is consistent with limited aprotic CO_2 reduction activity.

Under CO_2 saturation conditions in the presence of 0.1 M PhOH, a slight shift to positive potentials and large increase in current is observed which is consistent with the electrocatalytic CO_2 reduction reaction (CO_2RR) mediated by **1** (**Figure 3**, blue). At 0.1 M PhOH cross-tracing is apparent by CV, which disappears with increased PhOH concentrations (**Figure S9**) and at higher

scan rates (**Figure S10**). Additionally, similar CO₂RR reactivity in *N,N*-DMF is observed with H₂O as a proton source instead of PhOH (**Figure S11**).

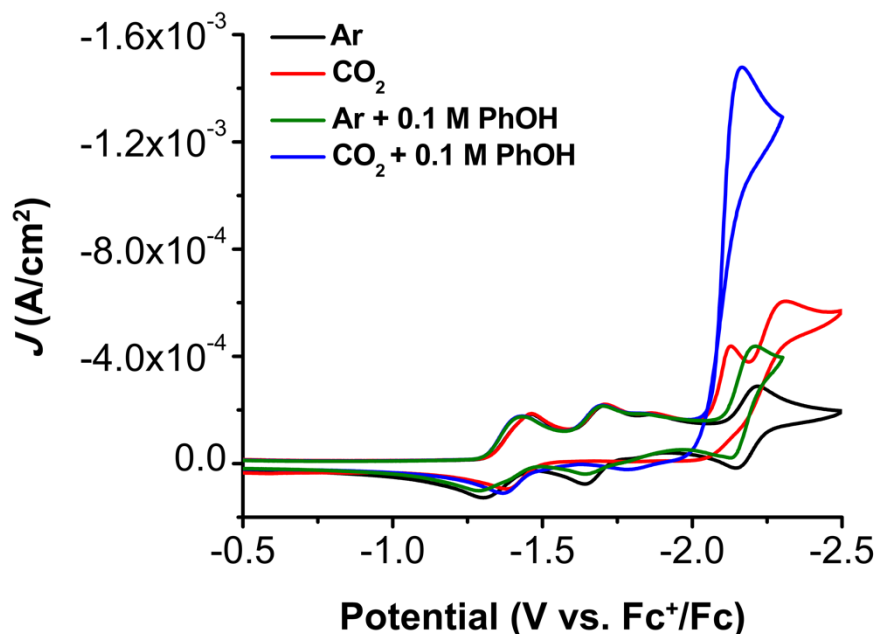


Figure 3. Comparison of CVs of 1.0 mM Cr(tpy^{tBuPhO})Cl₂ **1** under Ar and CO₂ saturation conditions with and without 0.1 M PhOH. Conditions: 0.1 M TBAPF₆/DMF; glassy carbon working electrode, glassy carbon rod counter electrode, Ag/AgCl pseudoreference electrode; referenced to Fc⁺/Fc internal standard; 100 mV/s scan rate.

Variable concentration studies suggest a linear relationship exists when the concentration of **1** and CO₂ are independently varied (**Figure S12** and **S13**, respectively). However, contrary to our previous report with Cr(^{tBu}dhbpy)Cl(H₂O), the catalytic current of the Cr(tpy^{tBuPhO})Cl₂ system is immediately saturated and does not increase with larger [PhOH] (**Figure S9**). This observation is distinct compared to the Cr(^{tBu}dhbpy)Cl(H₂O) system because it suggests that C–OH is no longer rate limiting in the catalytic mechanism with **1**.

Controlled potential electrolysis (CPE) experiments were performed at –2.3 V vs Fc⁺/Fc with **1** and 0.6 M PhOH under CO₂ saturation conditions (**Figure S14** and **Table S2**). These results demonstrated a 95±10% Faradaic efficiency for CO (FE_{CO}) for **1** over 11 turnovers operating at an

overpotential of 300 mV with no H₂ detected (**Table 1**). The turnover frequency (TOF) derived from this electrolysis experiment was $2.04 \times 10^4 \text{ s}^{-1}$, which is comparable to the TOF of $1.89 \times 10^4 \text{ s}^{-1}$ achieved by the dmbpy system.¹⁸⁻¹⁹ Additionally, a CPE experiment was performed with 2% H₂O in *N,N*-DMF as the proton source instead of PhOH (**Figure S15** and **Table S3**). With H₂O as a proton source in CPE experiments, Cr(tpy^{tbu}pho)Cl₂ maintained excellent selectivity for CO, with a FE_{CO} of 93±4% over 8 turnovers with no quantifiable amount of H₂ detected and a comparable TOF to conditions with PhOH present as the proton donor (**Table 1**).

Table 1. Results from CPE experiments under CO₂ saturation conditions.

Conditions	Potential (V vs Fc ⁺ /Fc)	FE _{CO}	TOF _{CPE} s ⁻¹	η (V)	TON _{CO}
[1] + PhOH	-2.3	95±10	2.04×10^4	0.3	11
[1] + H ₂ O	-2.3	93±4	1.12×10^4	0.41	7.5

* –[1] = Cr(tpy^{tbu}pho)Cl₂ **1**. PhOH = 0.6 M [PhOH]. Turnovers correspond to moles of electrons passed in coulometry studies divided by two to account for CO formation.

Mechanistic Insight via Computational (DFT) Analyses

In order to obtain additional insight, the reaction mechanism was interrogated by means of DFT calculations. CV data guided the initial investigation of the successive reduction events that the precatalyst undergoes to form the active species. Based on the proposal that solution equilibria involving the chloride ligands exists, five distinct redox events were examined for the overall three-electron reduction of complex **1**. Importantly, good correlation ($R^2 = 0.94$) between experimental redox potentials and computational results is obtained, suggesting the level of theory was appropriate for modeling this system (see **Table S4** and **Figure S16**). Note, in the shorthand notation used in the ensuing discussion to describe these calculations, the [tpypho]⁻ ligand has been eliminated for clarity and the other numbers are defined as follows $\overset{\text{multiplicity}}{\# \text{bound DMF}} \text{Cr}^{\text{charge}}$.

Unlike our previous study with the $\text{Cr}(\text{t}^{\text{bu}}\text{dhbpy})\text{Cl}(\text{H}_2\text{O})$ catalyst,¹⁸⁻¹⁹ the two-electron reduced species of $\text{Cr}(\text{tpy}^{\text{t}^{\text{bu}}}\text{pho})\text{Cl}_2$ is not reactive towards CO_2 . Consistent with experimental observations, it is the third overall reduction event (exp. $E_{1/2} = -2.18$ V vs Fc^+/Fc) that produces an overall monoanionic species capable of binding and activating CO_2 . Therefore, the active species of both catalysts have analogous overall charge (-1) and formal metal oxidation state (high-spin $\text{Cr}(\text{II})$), while differing in the number of ligand-centered reduction events (one for $\text{t}^{\text{bu}}\text{dhbpy}$, two for $\text{tpy}^{\text{t}^{\text{bu}}}\text{pho}$). The overall spin manifold is necessarily different: while $S = 3/2$ was found to be the preferential configuration for $[\text{Cr}(\text{II})(\text{t}^{\text{bu}}\text{dhbpy}^{\bullet})]^-$, the lowest-energy spin configuration for the active species for $[\text{Cr}(\text{II})(\text{tpy}^{\text{t}^{\text{bu}}}\text{pho}^{\bullet\bullet})]^-$ was an overall triplet ($S = 1$), with a terpyridine triplet diradical antiferromagnetically coupled to a high-spin $\text{Cr}(\text{II})$ center (**Figures 4A and S17A**). This finding is in good agreement with previous studies of terpyridine-containing electrocatalysts.²³⁻²⁴ Notably, the pentacoordinate solvent adduct ${}^3_1\text{Cr}^{-1}$ and tetracoordinate species ${}^3_0\text{Cr}^{-1}$ of the tpy-based catalyst are almost equally stable ($\Delta G = 0.2$ kcal/mol), the former being the lowest-energy configuration. Quintet (${}^5_0\text{Cr}^{-1}$) and septet (${}^5_0\text{Cr}^{-1}$) configurations were found at 3.0 and 6.8 kcal/mol above ${}^3_1\text{Cr}^{-1}$, respectively.

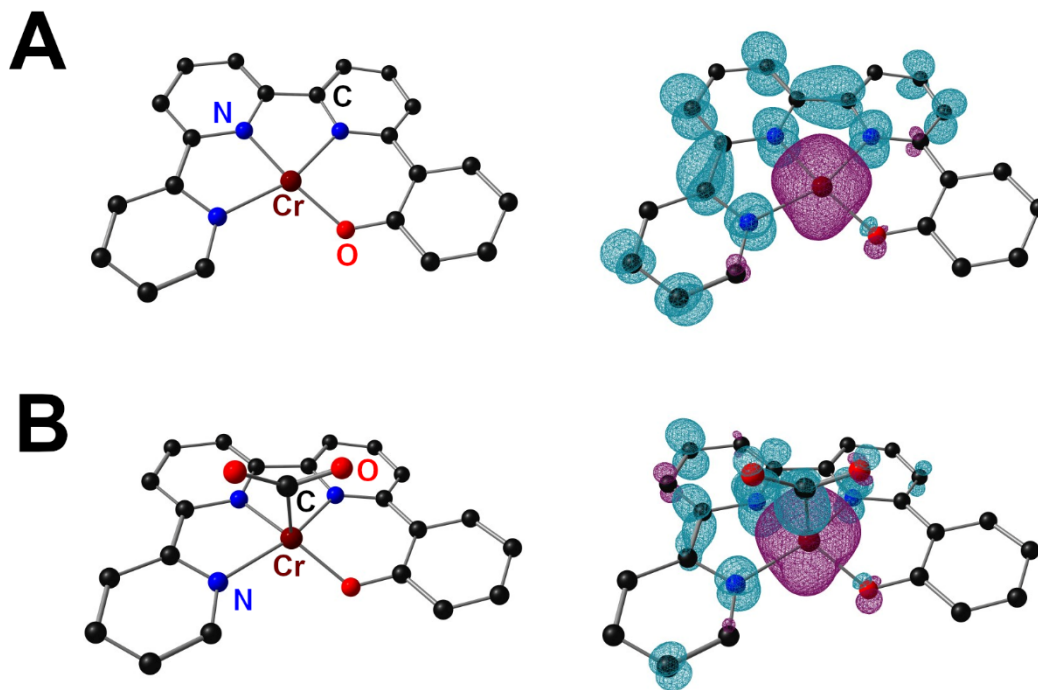


Figure 4. Molecular geometry and spin density plots of ${}^3_0\text{Cr}^{-1}$ (A) and ${}^3_0\text{Cr}(\text{CO}_2)^{-1}$ (B). For clarity, tbu groups and H atoms have been omitted.

From ${}^3_1\text{Cr}^{-1}$, the lowest-energy configurations for the transition state to bind CO_2 (no axial DMF, **Figure S18**) and the corresponding adduct (**Figure 4B** and **S17B**) were located in the $S = 1$ surface. The barrier for this catalyst was found to be higher (${}^3_0\text{TS1}^{-1}$, +12.2 kcal/mol) (**Figure 5**) than that located for CO_2 binding for the dhbpy counterpart (+10.0 kcal/mol). Interestingly, ${}^3_0\text{TS1}^{-1}$ presents a Cr–C bond distance of 2.35 Å, much shorter than the 2.64 Å found for the corresponding TS of the dhbpy system. This can be rationalized by analyzing the electronic structure of these species: for the dhbpy catalyst system, one of the two electrons that form the Cr–C bond is highly delocalized in a bpy-centered, metal-mixed π^* orbital in the TS geometry (see reference ¹⁹), conversely, for ${}^3_0\text{TS1}^{-1}$ both electrons have predominantly Cr–C σ -bond character (**Figure S18**). Furthermore, for the terpyridine-based catalyst CO_2 binding is

exergonic (${}^3_0\text{Cr}(\text{CO}_2)^{-1}$, -1.9 kcal/mol), in stark contrast with the endergonic binding calculated previously for the dhhpy system ($+4.7$ kcal/mol, **Figure S19**) and in good agreement with CV data for both systems. The electronic structure of the CO_2 adduct confirms the partial charge transfer from the reduced ligand: ${}^3_0\text{Cr}(\text{CO}_2)^{-1}$ presents a singly reduced tpy fragment (**Figure 4B**). The barrier for the thermodynamically favorable (-15.8 kcal/mol) formation of a metal hydride was located at $+20.7$ kcal/mol above ${}^3_1\text{Cr}^{-1}$, in agreement with the observed quantitative kinetic selectivity for CO (**Figure S19**).

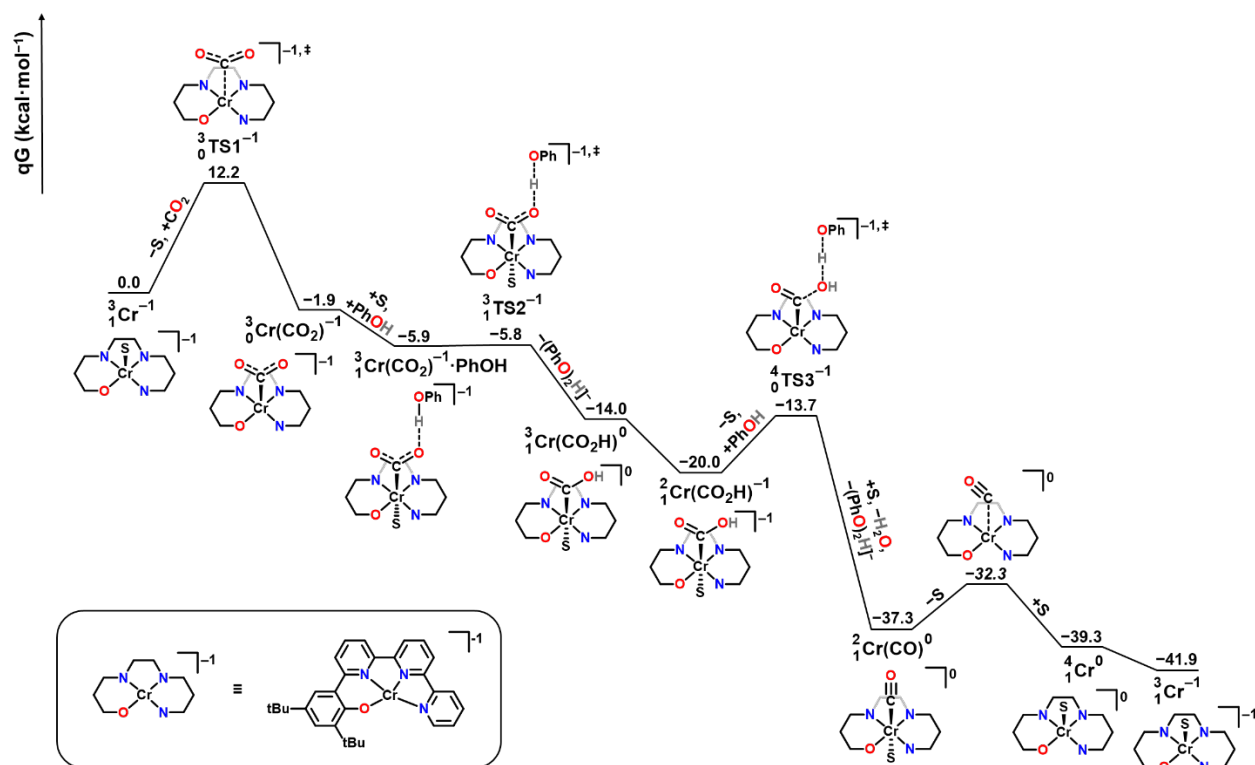


Figure 5. Free energy profile of the electrocatalytic CO_2RR cycle for **1**. Precatalyst reduction steps are omitted for clarity. S indicates a solvent adduct of *N,N*-DMF; procedure for the estimation of the barrier for CO release is described in the Supporting Information.

PhOH favorably binds to ${}^3_0\text{Cr}(\text{CO}_2)^{-1}$ to give ${}^3_1\text{Cr}(\text{CO}_2)\cdot\text{PhOH}^{-1}$ at -5.9 kcal/mol relative to ${}^3_1\text{Cr}^{-1}$, from which proton transfer has a barrier of only 0.1 kcal/mol (${}^3_1\text{TS2}^{-1}$, **Figure**

6A) and is thermodynamically favorable by 12.1 kcal/mol relative to ${}^3_0\text{Cr}(\text{CO}_2)^{-1}$ (PhOH homoconjugation in *N,N*-DMF and *N,N*-DMF binding to the product were taken into account^{19, 29}). The calculated reduction potential for the neutral six-coordinate hydroxycarbonyl complex ${}^3_1\text{Cr}(\text{CO}_2\text{H})^0$ is -2.12 V, leading to the doublet species ${}^2_1\text{Cr}(\text{CO}_2\text{H})^{-1}$ at potentials below the experimentally observed $E_{\text{cat}/2}$. The electronic structure of ${}^2_1\text{Cr}(\text{CO}_2\text{H})^{-1}$ is comprised of a doubly reduced, triplet diradical terpyridine and a high-spin Cr(III) complex (**Figure S20**). Despite hydrogen bonding of PhOH not being favorable for this species (+2.3 kcal/mol), the lowest-energy C–OH bond cleavage transition state (${}^4_0\text{TS3}^{-1}$, **Figure 6B**) lies only +6.3 kcal/mol above ${}^2_1\text{Cr}(\text{CO}_2\text{H})^{-1}$ in the $S = 3/2$ surface (**Figure 5**). This thermodynamically favorable step (–17.4 kcal/mol) does not appear to be rate-limiting and presents a notably lower barrier than the corresponding C–OH bond cleavage in the dhhpy system (10.4 kcal/mol). The lowest-energy spin configuration of the formed metal carbonyl is the doublet (${}^2_1\text{Cr}(\text{CO})^0$), arising from antiferromagnetically coupled electrons delocalized through the terpyridine backbone and the Cr–CO bond (**Figure S21**), from which we propose CO dissociation is facile and irreversible (**Figure S22**).^{18-19, 30-31}

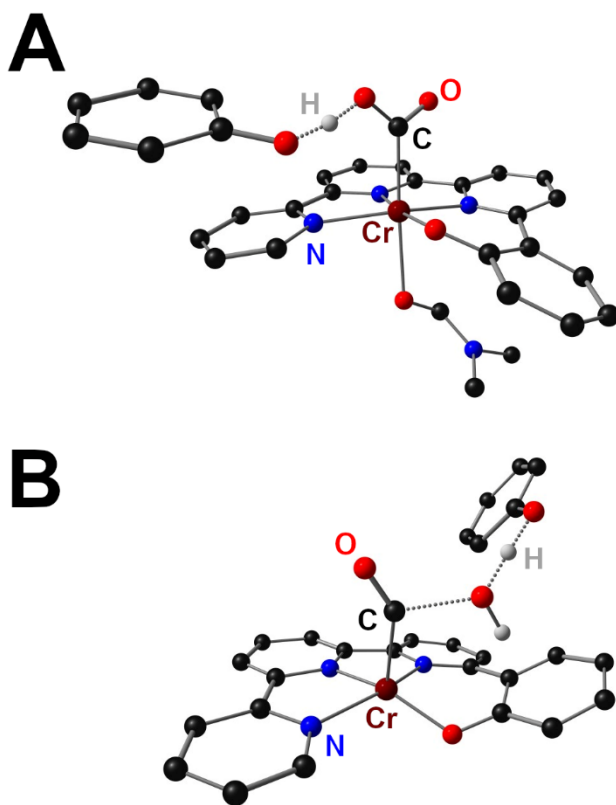


Figure 6. Molecular geometries of ${}^3_1\text{TS2}^{-1}$ (A) and ${}^4_0\text{TS3}^{-1}$ (B). For clarity, *tbu* groups and H atoms have been omitted.

Discussion

It is striking that the tpy-based Cr complex **1** largely achieves analogous activity, selectivity at comparable overpotentials to the bpy-based catalyst we have reported previously. Unlike the bpy-based catalyst, however, complex **1** binds CO₂ in the absence of a proton donor (**Figure 3**, red). Computational studies relevant to CO₂ binding suggest that, in comparison to the bpy-based complex, at the TS geometry the electrons forming the incipient Cr–C bond are relatively more localized on the metal and sigma-based, which could contribute to the comparatively heightened barrier for **1** than the bpy-based complex. Indeed, this is consistent with the need for charge reorganization from the doubly reduced tpy fragment to Cr being a key component. The formation of the product CO₂ adduct $[\text{Cr}(\text{tpy}^{\text{tbu}}\text{pho}^{\bullet})(\eta^1\text{-CO}_2)]^{-}$ is also significantly exergonic in contrast to

the endergonic formation of $[\text{Cr}(\text{t}^{\text{bu}}\text{dhbpy})(\eta^1\text{-CO}_2)]^-$. This trend is consistent with differences in operating potential: the catalytically relevant reduction potential of complex **1** ($E_{1/2} = -2.18$ V) is 0.23 V more negative than the bpy-based complex ($E_{1/2} = -1.95$ V).

The facile access to σ -basic character at Cr makes $[\text{Cr}(\text{II})(\text{tpy}^{\text{t}^{\text{bu}}}\text{pho}'')(\text{DMF})]^-$ more adept at interacting with the added proton donor PhOH than $[\text{Cr}(\text{II})(\text{t}^{\text{bu}}\text{dhbpy}')^-]$, which presents relatively more π -basic character. In CV studies with added PhOH under Ar saturation (**Figure 3**, green), a loss of reversibility occurs at the third reduction, consistent with an interaction between the Cr center and the proton donor. Conversely, the bpy-based Cr catalyst exhibited no comparable activity with added PhOH. DFT calculations show that the difference in transition state energy (ΔTS) between the barrier for protonation and CO_2 binding narrows across these two catalysts (ΔTS is 8.5 kcal/mol for $[\text{Cr}(\text{II})(\text{tpy}^{\text{t}^{\text{bu}}}\text{pho}'')(\text{DMF})]^-$, versus 20.2 kcal/mol for $[\text{Cr}(\text{II})(\text{t}^{\text{bu}}\text{dhbpy}')^-]$, **Figure S19**), consistent with the experimentally observed reactivity trends. Further, hydride formation from $[\text{Cr}(\text{II})(\text{t}^{\text{bu}}\text{dhbpy}')^-]$ is exergonic by 7.2 kcal/mol, whereas comparable hydride formation from $[\text{Cr}(\text{II})(\text{tpy}^{\text{t}^{\text{bu}}}\text{pho}'')(\text{DMF})]^-$ is even more thermodynamically favored, -15.8 kcal/mol. However, under electrocatalytic conditions **1** maintains quantitative selectivity for CO.

An additional consequence of the more negative potentials required for CO_2 binding by **1** appears to be relatively lower barriers for protonation to generate and protonate a hydroxycarbonyl intermediate ($\text{Cr-CO}_2\text{H}$) than those for the bpy-based analogue. Experimentally, saturation of the electrocatalytic current with added proton donor occurs at low concentrations for **1**, whereas a kinetic rate dependence was previously assessed for the bpy-based analogue. Computations again reflect these reactivity trends, suggesting that CO_2 binding is the rate-determining step for complex **1**, as opposed to the bpy-based catalyst, where C-OH bond cleavage was determined to be the rate-determining step.

Formation of a diradical state for the reduced ligand occurs again in $[\text{Cr(II)}(\text{tpy}^{\text{tbu}}\text{pho}^{\bullet\bullet})(\eta^1\text{-CO}_2\text{H})]^-$ $S = 3/2$, which precedes C–OH bond cleavage. During the formation of the Cr carbonyl and water co-products, one of these ligand-based unpaired electrons is transferred into the π -back-bonding scaffold of the forming CO ligand. For $[\text{Cr(II)}(\text{t}^{\text{bu}}\text{dhbpy}^{\bullet})(\eta^1\text{-CO}_2\text{H})]^-$ $S = 1$, a similar reaction pathway occurs, however, the barrier is relatively more significant and defines the rate of the process. It is likely that the increased redox-activity of tpy assists in diminishing the barrier of this chemical reaction step, since two charge equivalents are coupled to Cr and available for transfer, rather than one.

Conclusions

We report a new Cr-based electrocatalyst for the reduction of CO_2 to CO. Selective and stable Cr-based catalysts are underrepresented for the CO_2RR .⁴⁻⁶ Indeed, there are limited overall examples of the Cr/Mo/W triad showing either electrochemical or electrocatalytic activity.¹⁰⁻¹⁷ By expanding the polypyridyl core of the ligand, the ligand must be reduced twice to initiate the catalytic cycle, producing an active state which is best described as $[\text{Cr(II)}(\text{tpy}^{\text{tbu}}\text{pho}^{\bullet\bullet})]^-$ $S = 1$. The formation of a ligand-based diradical occurs again later in the catalytic cycle, when the intermediate prior to C–OH bond cleavage $\text{}^2_1\text{Cr}(\text{CO}_2\text{H})^{-1}$ is generated, demonstrating that coupling between the tpy-based ligand and Cr center alters the rate-determining step of the catalytic cycle. These results suggest that the ligand design principles used to develop selective, active, and stable late transition metal catalysts for the CO_2RR can be applied to metals much earlier in the transition metal series to create new categories of carbonyl ligand-free catalysts.

ASSOCIATED CONTENT

Supporting Information. Additional Material and Methods, CV, UV-vis, NMR, and electrochemical data is included in the SI. This material is available free of charge via the Internet at <http://pubs.acs.org>. Crystal data has been deposited with the CCDC: 2086769-2086770.

AUTHOR INFORMATION

Author Contributions. C.W.M. conceived and supervised the experiments; the manuscript was written by C.W.M., S.L.H. and J.J.M.; C.W.M. carried out the computational work and all experiments were carried out by S.L.H.; J.J.M. developed the ligand synthetic procedure utilized in this study and advised on computational methods. D.A.D. performed the crystallographic studies. All authors have given approval to the final version of the manuscript and declare no competing financial interest.

Corresponding Author. * - machan@virginia.edu

Funding Sources

University of Virginia.

ACKNOWLEDGMENT

The authors thank the University of Virginia for generous funding and institutional support.

References:

1. DuBois, D. L., Development of Molecular Electrocatalysts for Energy Storage. *Inorg. Chem.* **2014**, 53 (8), 3935-3960.
2. Das, B.; Thapper, A.; Ott, S.; Colbran, S. B., Structural features of molecular electrocatalysts in multi-electron redox processes for renewable energy – recent advances. *Sustainable Energy & Fuels* **2019**, 3 (9), 2159-2175.
3. IPCC *Global Warming of 1.5°C. An IPCC Special Report*; World Meteorological Organization: Geneva, Switzerland, 2018.
4. Jiang, C.; Nichols, A. W.; Machan, C. W., A look at periodic trends in d-block molecular electrocatalysts for CO₂ reduction. *Dalton Trans.* **2019**, 48, 9454-9468.

5. Francke, R.; Schille, B.; Roemelt, M., Homogeneously Catalyzed Electroreduction of Carbon Dioxide—Methods, Mechanisms, and Catalysts. *Chem. Rev.* **2018**, *118* (9), 4631-4701.
6. Kinzel, N. W.; Werlé, C.; Leitner, W., Transition Metal Complexes as Catalysts for the Electroconversion of CO₂: An Organometallic Perspective. *Angew. Chem., Int. Ed.* **2021**, (n/a), 10.1002/anie.202006988.
7. West, N. M.; Miller, A. J. M.; Labinger, J. A.; Bercaw, J. E., Homogeneous syngas conversion. *Coord. Chem. Rev.* **2011**, *255* (7), 881-898.
8. Kalck, P.; Le Berre, C.; Serp, P., Recent advances in the methanol carbonylation reaction into acetic acid. *Coord. Chem. Rev.* **2020**, *402*, 213078.
9. Hood, D. M.; Johnson, R. A.; Carpenter, A. E.; Younker, J. M.; Vinyard, D. J.; Stanley, G. G., Highly active cationic cobalt(II) hydroformylation catalysts. *Science* **2020**, *367* (6477), 542-548.
10. Clark, M. L.; Grice, K. A.; Moore, C. E.; Rheingold, A. L.; Kubiak, C. P., Electrocatalytic CO₂ reduction by M(bpy-R)(CO)₄ (M = Mo, W; R = H, tBu) complexes. Electrochemical, spectroscopic, and computational studies and comparison with group 7 catalysts. *Chem. Sci.* **2014**, *5* (5), 1894-1900.
11. Ramos Sende, J. A.; Arana, C. R.; Hernandez, L.; Potts, K. T.; Keshevarz-K, M.; Abruna, H. D., Electrocatalysis of CO₂ Reduction in Aqueous Media at Electrodes Modified with Electropolymerized Films of Vinylterpyridine Complexes of Transition Metals. *Inorg. Chem.* **1995**, *34* (12), 3339-3348.
12. Pickett, C. J.; Pletcher, D., Electrochemical reduction of Group 6 metal hexacarbonyls in aprotic solvents. *J. Chem. Soc., Dalton Trans.* **1976**, (8), 749-752.
13. Maia, L. B.; Fonseca, L.; Moura, I.; Moura, J. J. G., Reduction of Carbon Dioxide by a Molybdenum-Containing Formate Dehydrogenase: A Kinetic and Mechanistic Study. *J. Am. Chem. Soc.* **2016**, *138* (28), 8834-8846.
14. Tory, J.; Setterfield-Price, B.; Dryfe, R. A. W.; Hartl, F., [M(CO)₄(2,2'-bipyridine)] (M=Cr, Mo, W) Complexes as Efficient Catalysts for Electrochemical Reduction of CO₂ at a Gold Electrode. *ChemElectroChem* **2015**, *2* (2), 213-217.
15. Grice, K. A.; Saucedo, C., Electrocatalytic Reduction of CO₂ by Group 6 M(CO)₆ Species without “Non-Innocent” Ligands. *Inorg. Chem.* **2016**, *55* (12), 6240-6246.
16. Neri, G.; Donaldson, P. M.; Cowan, A. J., The Role of Electrode–Catalyst Interactions in Enabling Efficient CO₂ Reduction with Mo(bpy)(CO)₄ As Revealed by Vibrational Sum-Frequency Generation Spectroscopy. *J. Am. Chem. Soc.* **2017**, *139* (39), 13791-13797.
17. Mouchfiq, A.; Todorova, T. K.; Dey, S.; Fontecave, M.; Mougél, V., A bioinspired molybdenum–copper molecular catalyst for CO₂ electroreduction. *Chem. Sci.* **2020**, *11* (21), 5503-5510.
18. Hooe, S. L.; Dressel, J. M.; Dickie, D. A.; Machan, C. W., Highly Efficient Electrocatalytic Reduction of CO₂ to CO by a Molecular Chromium Complex *ACS Catal.* **2020**, *10*, 1146-1151.
19. Moreno, J. J.; Hooe, S. L.; Machan, C. W., DFT Study on the Electrocatalytic Reduction of CO₂ to CO by a Molecular Chromium Complex. *Inorg. Chem.* **2021**, *60* (6), 3635–3650.
20. Hooe, S. L.; Moreno, J. J.; Reid, A. G.; Cook, E. N.; Machan, C. W., Mediated Inner-Sphere Electron Transfer Induces Homogeneous Reduction of CO₂ via Through-Space Electronic Conjugation. **2021**, 10.26434/chemrxiv.14165951.v2.

21. Benson, E. E.; Sampson, M. D.; Grice, K. A.; Smieja, J. M.; Froehlich, J. D.; Friebe, D.; Keith, J. A.; Carter, E. A.; Nilsson, A.; Kubiak, C. P., The Electronic States of Rhenium Bipyridyl Electrocatalysts for CO₂ Reduction as Revealed by X-ray Absorption Spectroscopy and Computational Quantum Chemistry. *Angew. Chem., Int. Ed.* **2013**, 52 (18), 4841-4844.
22. Smieja, J. M.; Benson, E. E.; Kumar, B.; Grice, K. A.; Seu, C. S.; Miller, A. J. M.; Mayer, J. M.; Kubiak, C. P., Kinetic and structural studies, origins of selectivity, and interfacial charge transfer in the artificial photosynthesis of CO. *Proc. Natl. Acad. Sci.* **2012**, 109 (39), 15646-15650.
23. Derrick, J. S.; Loipersberger, M.; Chatterjee, R.; Iovan, D. A.; Smith, P. T.; Chakarawet, K.; Yano, J.; Long, J. R.; Head-Gordon, M.; Chang, C. J., Metal–Ligand Cooperativity via Exchange Coupling Promotes Iron- Catalyzed Electrochemical CO₂ Reduction at Low Overpotentials. *J. Am. Chem. Soc.* **2020**, 142 (48), 20489-20501.
24. Loipersberger, M.; Cabral, D. G. A.; Chu, D. B. K.; Head-Gordon, M., Mechanistic Insights into Co and Fe Quaterpyridine-Based CO₂ Reduction Catalysts: Metal–Ligand Orbital Interaction as the Key Driving Force for Distinct Pathways. *Journal of the American Chemical Society* **2021**, 143 (2), 744-763.
25. Keith, J. A.; Grice, K. A.; Kubiak, C. P.; Carter, E. A., Elucidation of the Selectivity of Proton-Dependent Electrocatalytic CO₂ Reduction by fac-Re(bpy)(CO)(3)Cl. *J. Am. Chem. Soc.* **2013**, 135 (42), 15823-15829.
26. Riplinger, C.; Sampson, M. D.; Ritzmann, A. M.; Kubiak, C. P.; Carter, E. A., Mechanistic Contrasts between Manganese and Rhenium Bipyridine Electrocatalysts for the Reduction of Carbon Dioxide. *J. Am. Chem. Soc.* **2014**, 136 (46), 16285-16298.
27. Cometto, C.; Chen, L.; Lo, P.-K.; Guo, Z.; Lau, K.-C.; Anxolabéhère-Mallart, E.; Fave, C.; Lau, T.-C.; Robert, M., Highly Selective Molecular Catalysts for the CO₂-to-CO Electrochemical Conversion at Very Low Overpotential. Contrasting Fe vs Co Quaterpyridine Complexes upon Mechanistic Studies. *ACS Catal.* **2018**, 8 (4), 3411-3417.
28. Newkome, G. R.; Hager, D. C.; Kiefer, G. E., Chemistry of heterocyclic compounds. Part 119. Synthesis of halogenated terpyridines and incorporation of the terpyridine nucleus into a polyetheral macrocycle. *J. Org. Chem.* **1986**, 51 (6), 850-853.
29. Nielsen, M. F.; Hammerich, O.; Rise, F.; Gogoll, A.; Undheim, K.; Wang, D. N.; Christensen, S. B., The Effect of Hydrogen Bonding between Methyl-Substituted Phenols and Dipolar Aprotic Solvents on the Rate Constants for. *Acta. Chem. Scan.* **1992**, 46, 883-896.
30. Labrum, N. S.; Chen, C.-H.; Caulton, K. G., A bis-Pyrazolate Pincer on Reduced Cr Deoxygenates CO₂: Selective Capture of the Derived Oxide by CrII. *Chem. - Eur. J.* **2019**, 25 (33), 7935-7940.
31. Perrotin, P.; Shapiro, P. J.; Williams, M.; Twamley, B., In Search of a Versatile Pathway to ansa-Chromocene Complexes. Synthesis and Characterization of the Highly Unstable ansa-Chromocene Carbonyl Complex Me₂C(C₅H₄)₂CrCO. *Organometallics* **2007**, 26 (7), 1823-1826.

TOC:

